Ref.TH.1385-CERN

MULTIPERIPHERAL AND POLYPERIPHERAL APPROACHES TO PIONIZATION

M. Bishari *)
CERN - Geneva

and

D. Horn **)
CERN - Geneva and Tel-Aviv University, Tel-Aviv

and

S. Nussinov **) ***)
Tel-Aviv University, Tel-Aviv

A B S T R A C T

Introduction of Regge trajectories in addition to the Pomeron, which appears in Mueller's approach to pionization, is shown to predict a small dip. The analysis is motivated by a multiperipheral approach. The question whether this approach may lead to an understanding of the peak in the pionic distribution or the asymmetry effect is discussed. A new (polyperipheral) approach based on the exchange of several chains is introduced in order to account for the observed effects. It leads naturally to Mandelstam cuts and is compared with a partonic picture.

---

*) On leave from the Weizmann Institute of Science, Rehovoth. Address from September 15 : Lawrence Radiation Laboratory, University of California, Berkeley.

**) Supported in part by the U.S. National Bureau of Standards.

***) Now at SUNY at Stony Brook.

Ref.TH.1385-CERN
13 August 1971

Let us begin with an intuitive derivation of Mueller's result [1] for pionization from a multiperipheral approach [2]. This model identifies the main bulk of the cross-section with diagrams of the type shown in Fig. 1. Breaking up the intermediate lines, one gets the production spectrum. In particular, by opening a single intermediate line, one obtains the representation of an inclusive cross-section indicated in Fig. 2. We are interested in the situation in which the outgoing particle of momentum p is almost equally separated (in CM longitudinal momentum space) from both the projectile (q_1) and the target (q_2). This corresponds to the pionization limit. If Fig. 1 can be associated with a representation of the two-body process (in the conventional Regge description), then Fig. 2 represents a sum of such factorized parts corresponding to specific Regge exchanges in the upper and lower parts.

The proceeding discussion of pionization will be based mainly on the above Mueller diagram and will be repeated at various degrees of complexity.

a) <u>The simple Pomeron-Pomeron limit</u>

The kinematics of the problem are simply described in the CM system. For simplicity, we discuss the case of pion production in proton-proton collision. We find then

$$q_1 = \left(\frac{W}{2}\,;\ 0,\ 0,\ q\right) \qquad \text{projectile, mass } M$$

$$q_2 = \left(\frac{W}{2}\,;\ 0,\ 0,\ -q\right) \qquad \text{target, mass } M \qquad (1)$$

$$p = \left(E\,;\ \vec{p}_T\,,\ p_L\right) \qquad \text{pion, mass } \mu$$

where $W = \sqrt{s}$. The invariant variables ν_1, ν_2 and ν are then defined by

$$M\nu = q_1 \cdot q_2 = \frac{W^2}{2} - M^2$$

$$M\nu_1 = q_1 \cdot p = \tfrac{1}{2} WE - qp_L \qquad (2)$$

$$M\nu_2 = q_2 \cdot p = \tfrac{1}{2} WE + qp_L$$

from which the following important relation follows

$$\frac{\nu_1 \nu_2}{m_T^2} = \frac{\nu}{2M} + \frac{E^2}{m_T^2} - \frac{1}{2} \tag{3}$$

where the transverse mass m_T is defined by

$$m_T^2 = \mu^2 + p_T^2 \tag{4}$$

The contribution of a double Regge exchange to an invariant inclusive cross-section has the form

$$E \frac{d^3\sigma}{d^3p} = \frac{\nu_1^{\alpha_1} \nu_2^{\alpha_2}}{\nu} f_{\alpha_1,\alpha_2}(m_T) \tag{5}$$

Strictly speaking, Mueller's analysis yields

$$E \frac{d^3\sigma}{d^3p} = \frac{\nu_1^{\alpha_1} \nu_2^{\alpha_2}}{\nu} g_{\alpha_1,\alpha_2}(\varphi) \tag{6}$$

In terms of the scaling variable $x = \frac{2p_L}{W}$ one finds in the limit $\nu_1, \nu_2 \gg \mu$ that

$$\frac{\mu^2}{M}(1+\cos\varphi)^{-1} \approx \frac{\nu_1 \nu_2}{\nu} = \frac{m_T^2}{2M} + \frac{Mx^2}{2} + \frac{m_T^2}{2\nu} \tag{7}$$

Choosing $x \sim 0.05$ and $m_T \gtrsim 0.3$ GeV, we see that Eq. (6) reduces effectively to Eq. (5) since the correction is negligible. We chose the variables ν_1, ν_2 and ν to have the dimensions of masses in order to compare the situation here with conventional Regge analysis of two-body scattering amplitudes.

The pionization limit corresponds to small x and large ν, so that by virtue of Eq. (2) and (3) we are interested in

$$\nu_1 \approx \nu_2 \approx \sqrt{\frac{m_T^2 \nu}{2M}} \tag{8}$$

The limit $\nu \to \infty$ corresponds, therefore, to $\nu_1, \nu_2 \to \infty$. The dominant contribution of the form (5) will then be given by $\alpha_1 = \alpha_2 = \alpha_p(0) = 1$ (the Pomeron-Pomeron limit)

$$E \frac{d^3\sigma}{d^3p} = f(m_T) \tag{9}$$

This famous "$\frac{dp}{E}$ spectrum", originally derived in the framework of the multiperipheral model of Amati, Fubini and Stanghelini [2] corresponds to the wee partons in Feynman's language [3], and it is satisfying that Mueller's analysis also yields it rather naturally as the two Pomeron contribution.

A pionization formula that is based on two Pomeron exchanges, carries with it more information than just the result (9), if one invokes the assumption of factorization of the Pomeron. This leads to the result

$$\frac{1}{\sigma_T} E \frac{d^3\sigma}{d^3p} = F(m_T) \tag{10}$$

where $F(m_T)$ is now a universal function independent of the incoming particles. Such factorization assumptions are known to work well in the fragmentation [4] and diffraction [5] regions.

Available data in the energy ranges of 10-30 GeV do not seem to support the universality relation (10) nor do they exhibit a scaling plateau. Conventional shapes are of a Gaussian type in rapidity and recent comparison of πp reactions at 8 and 16 GeV indicate an increase of the distribution with energy [6]. This suggests that the simple Pomeron-Pomeron limit does not provide us with an adequate description of the presently available data.

b) Corrections due to non-Pomeron exchanges

The most obvious correction to Eq. (9) comes from exchanges of non-Pomeron Regge trajectories with $\alpha(0) < 1$. This seems particularly necessary since the energies ν_1 and ν_2 are relatively small, of the order of 1-2 GeV for presently available data. Contributions of non-leading trajectories (P', ρ etc.) are likely to be important and, if we rely on an analogy with π N collisions, they may be comparable with the diffractive Pomeron component. Note, in particular, that ν_1 and ν_2 are proportional to m_T in Eq. (8) and, therefore, the deviations from the asymptotic Pomeron-Pomeron limit are expected to be enhanced in the smaller m_T region. One indeed observes that the distributions in x are more peaked for lower m_T values. The introduction of non-leading trajectories modifies the $x \approx 0$ distribution and leads also to well defined expectations for differences between distributions of different pions [7].

The analogy with two-body scattering amplitudes leads to the following expression

$$E\frac{d^3\sigma}{d^3p} \approx \frac{1}{\nu}(\nu_1+a\nu_1^{\alpha})(\nu_2+a\nu_2^{\alpha})\,f(m_T) \qquad (11)$$

The parameter a, which in general can also depend weakly on m_T, is expected to be positive. This follows directly from the analogy with two-body scattering amplitudes where it is known experimentally that the cross-sections tend to decrease towards their asymptotic values. There is a rather natural explanation of this fact in terms of a "two component" theory of the total two-body cross-sections [8]. According to this theory, the resonances contribute positively to the usual Regge exchanges and the positive background contribution builds up the Pomeron exchange. We extend this hypothesis to the two subprocesses of Fig. 3. This figure is a pictorial representation of a general pionization process. The two subprocesses involve forward scattering of virtual particles which one, therefore, also expects to decrease towards their asymptotic value. This is manifested by a positive a in Eq. (11).

The positivity of a together with the fact that $\alpha < 1$ and the constraint on the product $\nu_1\nu_2$, Eq. (3), means that the point $x = 0$ will actually be a (weak) minimum of $E\frac{d^3\sigma}{d^3p}$ of Eq. (11). In addition, it implies that the value at $x = 0$ decreases towards its asymptotic value. Both of these trends are in contradiction with the data quoted before. We see, therefore, that the addition of the lower Regge exchanges did not lead to a consistency with present data. In the forthcoming sections, we will discuss various other alternatives that may shed light on this question. In the meantime, let us assume that Eq. (11) is applicable in some higher energy range and investigate its consequences in some more detail.

To see the effects of Eq. (11) we want to stay in the region where $\nu_1\nu_2 \approx (m_T^2/2M)\nu$ and to be able also to allow $\nu_1/\nu_2 \ll 1$. The first condition leads to [see Eq. (7)] $x^2 \ll m_T^2/M^2$. The second condition is met when $E-p_L$ is small [see Eq. (2)], namely $p_L^2 \gg m_T^2$ and $x^2 \gg (2m_T/W)^2$. The combined effect of the two defines, therefore, the border region between fragmentation and pionization where effects of Eq. (11) should be felt :

$$\left(\frac{2m_T}{W}\right)^2 \ll x^2 \ll \left(\frac{m_T}{M}\right)^2 \qquad (12)$$

It follows then from Eq. (2) that

$$\nu_1 \approx \frac{m_T^2}{2Mx} \qquad \nu_2 \approx x\nu \qquad (13)$$

which means that

$$\frac{\nu_1^{\alpha_1}\nu_2^{\alpha_2}}{\nu} = \left(\frac{m_T^2}{2M}\right)^{\alpha_1} \nu^{\alpha_2-1} x^{\alpha_2-\alpha_1} \qquad \text{for} \qquad \frac{2m_T}{W} < x < \frac{m_T}{M} \tag{14}$$

This is clearly asymmetric since we chose $\nu_1/\nu_2 \ll 1$ thus approaching fragmentation of the projectile. We learn that, as expected, the leading contribution, achieved when $\alpha_2 = 1$, is scaling in x. Hence the terms of Eq. (11) that survive in the scaling limit ($\alpha_2 = 1$) will be

$$E\frac{d^3\sigma}{d^3p} \approx f(m_T) + x^{1-\alpha} g(m_T) \tag{15}$$

which, with positive values for $g(m_T)$, leads to a decrease towards $x = 0$. The above quoted range of x was the one necessary for the mathematical manipulations. In order to investigate when a Regge term may be assumed to dominate the physical amplitude, let us require *)

$$\nu_1 > M \qquad\qquad \nu_2 > M \tag{16}$$

which leads to

$$\frac{M}{\nu} < x < \frac{m_T^2}{2M^2} \tag{17}$$

The upper limit of Eq. (17) is lower than that of Eq. (12) and leads characteristically to $x < 0.05$. The lower limit of Eq. (17) is at high energies below the lower limit of Eq. (12). Hence, we may expect to see such effects when $2m_T/W \ll m_T^2/2M^2$ or $W \gg 4M^2/m_T$, which is a condition that can be met by the ISR and NAL machines.

c) Effects of the exchange mechanism

If we use Fig. 3 as the guide for our study, then the relevant variables are $k_1 \cdot q_1$ and $k_2 \cdot q_2$ rather than $p \cdot q_1$ and $p \cdot q_2$ respectively. Clearly k_1 and k_2 cannot appear in the final formula since they are integrated upon. Therefore, the distribution has to be given in terms of ν_1 and ν_2, the observed energy variables. Within the framework of the multiperipheral model, this does not pose a severe problem because the ratio $k_1 \cdot q_1 / p \cdot q_1$ peaks around a central value which depends on the parameters of the model [Ref. 9].

*) It should be pointed out that the unobserved invariant masses of the upper and lower clusters in Fig. 3 are more relevant to the question of asymptotics that the observed ν_1 and ν_2. In the most optimal configurations of a multiperipheral model those m^2 values are proportional to the respective ν values. This proportionality constant may, however, be small.

In looking for possible deviations from the flat distributions predicted by the multiperipheral model, it may seem worthwhile to evaluate directly the absorptive loop diagram shown in Fig. 3. In doing so, we assume that the upper and the lower blobs are given simply by Pomeron exchange. The explicit (unknown) forms of the propagators $D_i(k_i^2)$ enter into the resulting loop integral. These calculations are rather involved. Bali, Pignotti and Steele [10], who studied this problem, have made the simplifying approximation that the propagator falls off exponentially like $e^{-\Omega|k_i^2|/2}$. This leads to an $e^{-\Omega|t_1+t_2|}$ term in the integrand where $t_i = k_i^2$. Furthermore, they argued that the strong damping factor allows us to conclude that the main features of the distribution are given by $e^{-\Omega|t_1+t_2|_{min}}$. For fixed $s_i = (k_i+q_i)^2$, taken for simplicity to be equal $s_1 = s_2 = s'$, this minimum turns out to be

$$|t_1+t_2|_{min} = (s'-M^2)x + s'x^2 + \frac{p_T^2}{2} \qquad (18)$$

which leads to the following distribution *)

$$\exp\left\{-\Omega\left[(s'-M^2)|x| + s'x^2 + \frac{p_T^2}{2}\right]\right\} I_1(p_T^2, x, s') \qquad (19)$$

where I_1 is a slowly varying function of its arguments. Allowing s_1 and s_2 to vary over all the kinematical region, one finds that the over-all minimum of $|t_1+t_2|$ occurs at threshold $s_1 = s_2 = M^2$. In this case, the linear term in x in Eq. (18) drops and one is left with

$$E\frac{d^3\sigma}{d^3p} = \exp\left\{-\Omega\left[M^2x^2 + \frac{p_T^2}{2}\right]\right\} I_2(p_T^2, x) \qquad (20)$$

which is the result of Bali et al. [10]. This is rather strange since one would not like to ascribe the main bulk of the pionization phenomenon to the process $pp \to NN\pi$. In reality, we expect each of the two clusters of Fig. 3 to include many pions in addition to the nucleon. Many of these pions are also emitted with low CM momenta. Consequently s_1 and s_2 are expected to be significantly higher than M^2. Returning now to Eq. (19) and choosing, e.g., $s' = 3M^2$ we find it difficult to fit with the single parameter Ω both the p_T as well as the x behaviours. Nevertheless, the functional form of Eq. (19) has some satisfying aspects - it provides for the peaking of the distribution around $x = 0$. The exponential cut-off in t, which is the main ingredient in this analysis, is strongly suggestive of some more complicated structure than the one implicit in a simple ABFST model. Such a modification of a simple propagator corresponds presumably to multiple-exchange diagrams. This may suggest that such diagrams should be taken into account in order to gain a better understanding of the pionization phenomenon.

*) For pions with finite masses the distribution is smooth at $x = 0$.

d) Unitarity corrections to the ABFST model

The prediction of the pionization plateau in the multiperipheral models in the limit of large numbers of particles produced [9]. In such a model, based on pion exchanges and $\pi - \pi$ resonance production, the relevant number is the number of resonances produced. This number cannot be larger than 3-4 at conventional machine energies. One should, therefore, expect strong corrections (end effects). We comment here on one particular such effect [*] due to unitarity corrections [2]. In all likelihood this is not the main end effect, but it leads to interesting results.

To understand this effect, let us first compare Figs. 4a and 4b. Fig. 4a corresponds to a simple ideal multiperipheral diagram and Fig. 4b shows a diffractive correction. The contribution of Fig. 4b is suppressed by $\sigma_{el}(\pi\pi)/\sigma_T(\pi\pi)$ compared to Fig. 4a. This ratio should be evaluated at the relevant $\pi\pi$ energies $(k_i - k_{i+m})^2$. Diffractive corrections of the type of Fig. 4c contribute to end effects. Here a factor of $\sigma_{el}(\pi N)/\sigma_T(\pi N)$ should be introduced. In analogy with the relation $\sigma_{el}(NN)/\sigma_T(NN) > \sigma_{el}(\pi N)/\sigma_T(\pi N)$ (values are $0.25 > 0.17$ at 15 GeV) we may expect also $\sigma_{el}(\pi N)/\sigma_T(\pi N) > \sigma_{el}(\pi\pi)/\sigma_T(\pi\pi)$ which would then mean that diagrams 4c are more important than diagrams 4b. The effect of any diffractive correction is to cause a depletion in an ideally flat distribution. If $\sigma_{el}(\pi N)/\sigma_T(\pi N) > \sigma_{el}(\pi\pi)/\sigma_T(\pi\pi)$ we expect a stronger depletion near the ends. Obviously, this cannot explain the whole of the pionization peak effect since diagram 4d, relevant to πN scattering, is not expected to cause a net depletion in the direction of the incoming pion, whereas experimentally one observes pionization peaks in both NN and πN collisions. It is amusing to note that the above discussion suggests an asymmetry in the distribution of the outgoing pions in πN collisions. In particular, one would expect more pions to emerge in the incoming pion's direction rather than in the nucleon's direction. This is qualitatively in agreement with the observed asymmetry in the pionic distributions [11].

e) Polyperipheral model

Our discussion so far was based on multiperipheral models and on factorizing reggeized Mueller amplitudes. In this section we consider as a natural generalization the "polyperipheral diagrams" involving several ladder exchanges as indicated in Fig. 5.

Even without any detailed estimates, it is obvious that such diagrams will create a concentration of pions in the centre-of-mass. In order to see this, let us assume for simplicity a symmetrical collision, i.e., $k_1 = k_1'$, $k_2 = k_2'$ etc. Each chain (i) will then yield n_i pions in a uniform distribution of $E\, d^3\sigma/d^3p$ over a range $(-k_i, k_i)$ in the CM. In terms of the scaling variable x, each polyperipheral diagram leads to a superposition of flat spectra, all with the same height. Each such flat distribution extends only over a range $\pm k_i/P_{max}$ rather than ± 1. If we use as a representative of all polyperipheral diagrams with m chains the diagram with m equal chains we get

---

[*] We would like to acknowledge a useful discussion with S. Fubini on this point.

$$E\frac{d\sigma}{d\vec{p}} \approx \sum_{m=1}^{m_{max}} c(m)\lambda^m m\,\theta\left(x+\tfrac{1}{m}\right)\theta\left(x+\tfrac{1}{m}\right) \qquad (21)$$

where λ is some effective coupling parameter and $c(m)$ is a combinatoric weight representing the effect of all other diagrams with m chains. Obviously, the important remaining task is to try and estimate the relative importance of diagrams with $m > 1$ terms in Eq. (21).

When diagrams of the type shown in Fig. 5 are closed by multiplying them by their conjugates, one obtains Mandelstam cuts [12] in the elastic amplitude. This is shown diagramatically in Fig. 6. It is generally believed that the contribution of such cuts to the total cross-section is suppressed by $1/\ln s$ factors compared to the (Regge) pole diagrams. Even if their effect on the total cross-section is relatively small, their relative importance in the inclusive distribution is strongly enhanced by the factor of m in Eq. (21).

The simple multiperipheral model leads not only to a uniform distribution but also to clear correlations between the quantum numbers of neighbouring particles on the chain. Preliminary searches for such correlations were unsuccessful [13]. A polyperipheral diagram would destroy such correlations since neighbouring particles in momentum space may emerge from different chains. In addition, it also invalidates a factorized reggeized Mueller approach such as discussed in Sections a) and b) above.

An alternative motivation for the introduction of polyperipheral diagrams is a space-time picture viewing the colliding particles as extended objects [14] of radius r. This is intuitively suggested by the fact that the diagram 5 corresponds to a dissociation of the incoming particles into constituents which then scatter simultaneously and independently. The particle structure corresponds to the blobs in Fig. 5. The relative importance of higher order polyperipheral diagrams depends on the relative importance of this structure.

The "multiperipheral model" does, to a certain extent, deemphasize the structure of the colliding particles. The latter is reflected only in the (a priori unknown) residue functions $\beta(t)$ of the Regge pole exchanges. A multiperipheral chain with n links, based on Feynman diagrams with exchanges of particles of average mass μ, leads to a diffraction radius given by $\langle b^2\rangle \propto n/\mu^2$. This result [15] follows from the fact that each propagator corresponds in transverse configuration space to an average separation of $1/\mu$. The various propagators are uncorrelated in direction thus leading to the above random walk result. Since, furthermore, within the multiperipheral model the average chain length (or the average multiplicity) $\bar{n}$ increases logarithmically with incident energy, one finds

$$b^2 \approx \bar{n}\, b_0^2 \propto b_0^2 \ln s \qquad b_0 \propto \frac{1}{\mu} \qquad (22)$$

Experimental data [16] indicate that the pp diffraction peak does not shrink as fast as the multiplicity $\bar{n}$ grows. This suggests that the multiperipheral chain is not the sole reason for the range of interactions. One could perhaps regard the colliding particles as extended objects of radius $r > b_0$, the constituents (partons) of which interact via multiperipheral chains as in the polyperipheral diagram.

The strength of a double vs. single exchange of multiperipheral chains is proportional to r^2/b^2. This is evident if we realize that the probability of the second chain, that spreads in a range of b, to terminate in a particle of radius r is given by the ratio of the two areas. This corresponds to the 1/lns suppression factor of the Regge cuts. We see, however, that if r and b are comparable, as the small observed shrinkage suggests, the cuts may in practice be very big.

At this point, let us depart from the diagrammatical approach and concentrate on a space-time picture. Let us define a distribution of partons in a three dimensional space spanned by $\vec{b}$, the transverse vector in configuration space measured from the centre of the particle, and p - a longitudinal momentum. The distribution $\rho_A(\vec{b},p)$ refers to particle A and has the properties

$$\int \rho_A(\vec{b},p)\, d^2b\, dp = N_A \qquad \int p\,\rho_A(\vec{b},p)\, d^2b\, dp = q_A \tag{23}$$

where q_A is the longitudinal momentum of particle A and N_A is the average number of partons in particle A. The density of partons projected on the transverse plane is given by

$$n_A(\vec{b}) = \int \rho_A(\vec{b},p)\, dp \tag{24}$$

We assume that the collision of particles A and B consists of essentially independent collisions between partons belonging to A and B. The interactions between the partons are described by a propagator g. The total cross-section is then given in terms of a convolution

$$\eta(b_{AB}) = \int d^2b_A\, n_A(\vec{b}_A)\, d^2b_B\, n_B(\vec{b}_B)\, g(\vec{b}_A - \vec{b}_B + \vec{b}_{AB}) \tag{25}$$

by

$$\sigma_T(AB) = \int 4\pi b\, db\, (1 - e^{-\eta(b)}) \tag{26}$$

b_{AB} in Eq. (25) is the impact parameter between the centres of the two particles A and B. The polyperipheral approach leads to a propagator g that is built from a multiperipheral chain and is, therefore, slowly varying with energy. In a usual pure geometrical approach [14] one assumes this interaction to be energy independent and short ranged. In the limit of small η one can expand the exponent in Eq. (26) to obtain

$$\sigma_T(AB) \approx \int 4\pi b\, db\, \eta(b) = G N_A N_B \tag{27}$$

This corresponds then physically to the neglect of mutual shadowing effects. Diagrammatically such shadow effects correspond to unitarity corrections (e.g., AFS cuts) in which the same partons scatter several times. Such corrections would spoil the factorization property of Eq. (27). It should be pointed out that such AFS shadow terms cannot be obtained by a closure of polyperipheral diagrams.

The collision of a parton from A with a parton from B may be either elastic or inelastic. The partons which scattered elastically, as well as those that did not scatter at all, form new distributions ρ_{A^*} and ρ_{B^*} which constitute the two fragmentation systems. Inelastic scatterings lead to formation of meson clouds, thus building the pionization region. A consequence of Eq. (23) is that each parton carries, on the average, a longitudinal momentum of $\frac{q}{N}$. The pionization distribution in longitudinal momentum will peak symmetrically at the CM system of the parton pairs. This is the frame in which

$$R = -\frac{q_A}{q_B} = \frac{N_A}{N_B} \tag{28}$$

In the approximation of Eq. (27) one furthermore finds that this frame is characterized by

$$R \approx \frac{\sigma_T(AX)}{\sigma_T(BX)} \tag{29}$$

This last result is reminiscent of the "quark derivation" [11] of the asymmetry parameter R. Our result, however, does not necessitate small numbers of partons. Therefore, we do not get an a priori fixed value like $R = \frac{3}{2}$ but, instead, a connection of the type (29).

ACKNOWLEDGEMENTS

We would like to thank S. Fubini, Y. Goren, M. Kugler, L. Susskind and G. Veneziano for many helpful discussions. We would like also to acknowledge the hospitality of the Theoretical Study Division of CERN.

REFERENCES

1) A.H. Mueller, Phys.Rev. D2, 2963 (1970).

2) L. Bertocchi, S. Fubini and M. Tonin, Nuovo Cimento 25, 626 (1962) ; D. Amati, S. Fubini and A. Stanghellini, Nuovo Cimento 26, 896 (1962).

3) R.P. Feynman, Phys.Rev.Letters 23, 1415 (1969) and in "High Energy Collisions", ed. by C.N. Yang et al., (Gordon and Breach, New York, 1969), p. 237.

4) M.S. Chen et al., Phys.Rev.Letters, 26, 1585 (1971).

5) P.G.O. Freund, Phys.Rev.Letters 21, 1375 (1968).

6) ABBCCHW collaboration, paper submitted to the Amsterdam Conference (1971).

7) H.D.I. Abarbanel, Phys.Letters B34, 69 (1971).

8) P.G.O. Freund, Phys.Rev.Letters 20, 235 (1968) ; H. Harari, Phys.Rev.Letters 20, 1395 (1968).

9) S. Fubini in Scottish Universities Summer School 1963, ed. by R.G. Moorhouse, Oliver and Boyd (1964), p. 259.

10) N.F. Bali, A. Pignotti and D. Steele, Phys.Rev. D3, 1167 (1971). See also L. Caneschi, Phys.Rev. D3, 2865 (1971) whose conclusions are in accord with our discussion in Section c).

11) J.W. Elbert, A.R. Erwin and W.D. Walker, Phys.Rev. D3, 2042 (1971). For summary of various R values, see paper submitted by ABBCCHW collaboration to the Amsterdam Conference.

12) S. Mandelstam, Nuovo Cimento 30, 1127 and 1148 (1963).

13) J. Grunhaus and S. Nussinov, unpublished.

14) T.T. Chou and C.N. Yang, Phys.Rev. 170, 1591 (1968).

15) See e.g., J.D. Bjorken, invited talk at the International Conference on Duality and Symmetry in Hadron Physics, Tel Aviv (1971).

16) M. Holder et al., Phys.Letters 35B, 355 (1971).

FIGURE CAPTIONS

Figure 1 :

The multiperipheral approach.

Figure 2 :

The pionization diagram.

Figure 3 :

The loop in the pionization diagram.

Figure 4 :

Unitarity effects on multiperipheral diagrams.

Figure 5 :

A polyperipheral diagram.

Figure 6 :

A Mandelstam cut produced by the polyperipheral diagram of Fig. 5.

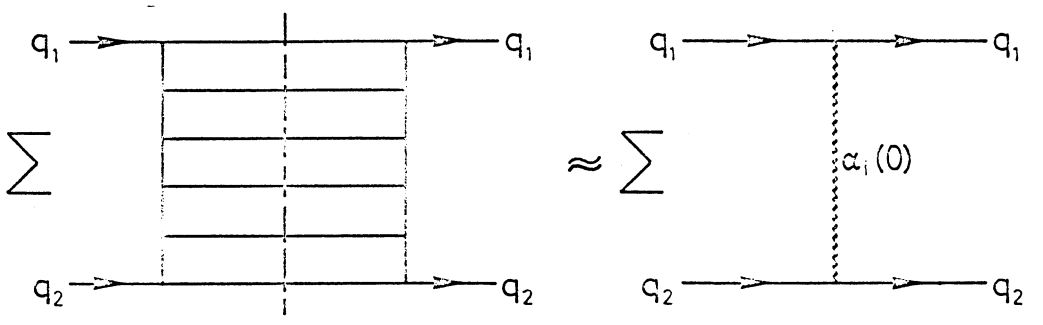

FIG.1

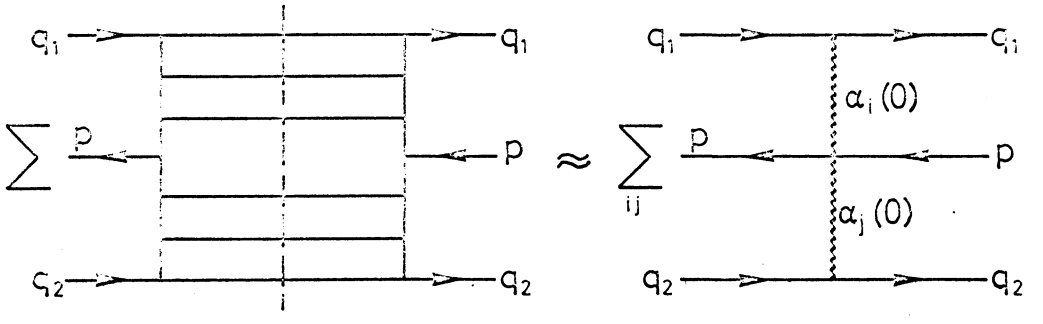

FIG. 2

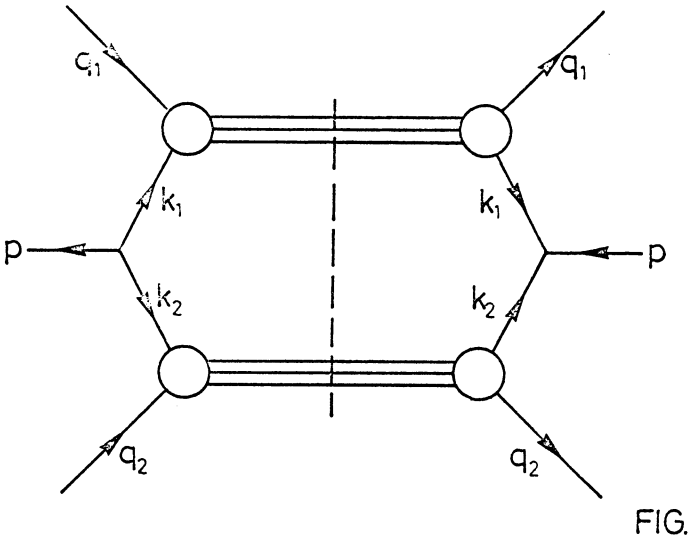

FIG. 3

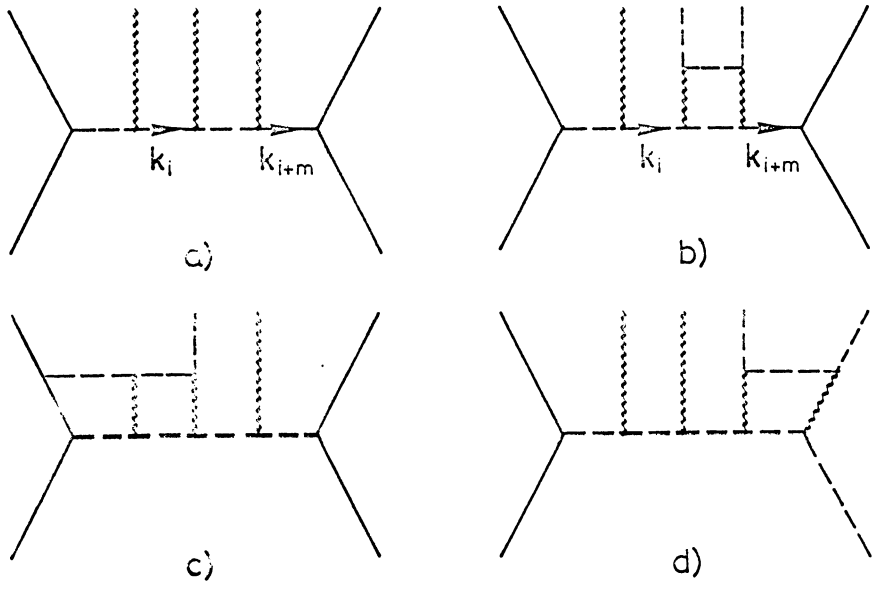

FIG. 4

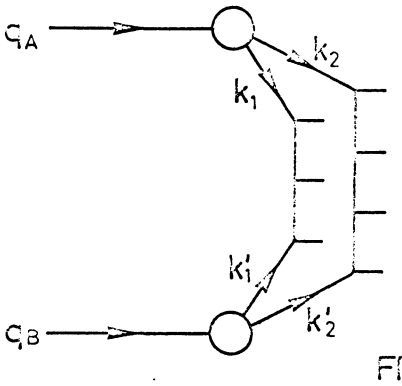

FIG. 5

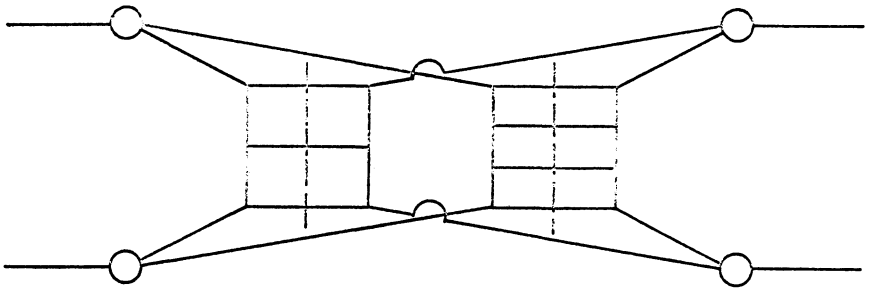

FIG. 6